THE ASTROPHYSICAL JOURNAL, 515:726–737, 1999 April 20
© 1999. The American Astronomical Society. All rights reserved. Printed in U.S.A.

ROSSI X-RAY TIMING EXPLORER OBSERVATION OF CYGNUS X-1. III. IMPLICATIONS FOR COMPTON CORONA AND ADVECTION-DOMINATED ACCRETION FLOW MODELS

MICHAEL A. NOWAK,[1] JÖRN WILMS,[2] BRIAN A. VAUGHAN,[3] JAMES B. DOVE,[1,4] AND MITCHELL C. BEGELMAN[1,5]
Received 1998 May 27; accepted 1998 December 1

ABSTRACT

We have recently shown that a "sphere + disk" geometry Compton corona model provides a good description of *Rossi X-Ray Timing Explorer* (*RXTE*) observations of the hard/low state of Cygnus X-1. Separately, we have analyzed the temporal data provided by *RXTE*. In this paper we consider the implications of this timing analysis for our best-fit "sphere + disk" Comptonization models. We focus our attention on the observed Fourier frequency-dependent time delays between hard and soft photons. We consider whether the observed time delays are created in the disk but are merely reprocessed by the corona, created by differences between the hard and soft photon diffusion times in coronae with extremely large radii, or are due to "propagation" of disturbances through the corona. We find that the time delays are most likely created directly within the corona; however, it is currently uncertain which specific model is the most likely explanation. Models that posit a large coronal radius (or equivalently, a large advection-dominated accretion flow region) do not fully address all the details of the observed spectrum. The Compton corona models that do address the full spectrum do not contain dynamical information. We show, however, that simple phenomenological propagation models for the observed time delays for these latter models imply *extremely* slow characteristic propagation speeds within the coronal region.

Subject headings: accretion, accretion disks — black hole physics — stars: coronae — stars: individual (Cygnus X-1) — X-rays: stars

1. INTRODUCTION

In a previous paper (Dove et al. 1998, hereafter Paper I) and in a companion paper to this work (Nowak et al. 1998a, hereafter Paper II) we presented an analysis of a 20 ks *Rossi X-Ray Timing Explorer* (*RXTE*) observation of the black hole candidate Cygnus X-1. Using self-consistent numerical models of a hot spherical corona surrounded by a cold, geometrically thin disk, we were able to describe successfully the spectrum of Cyg X-1 over a broad range in energy, 3–200 keV (Paper I; see also Dove et al. 1997b). We derived an optical depth for the spherical corona of $\tau = 1.6 \pm 0.1$ and an average temperature of $kT = 87 \pm 5$ keV (reduced χ^2 for the fit was 1.56; Paper I).

Timing analysis (Paper II) showed that our observation of the hard state of Cyg X-1 was similar to previous hard state observations of this object (Miyamoto & Kitamoto 1989; Belloni & Hasinger 1990a, 1990b; Miyamoto et al. 1992); however, we were able to extend our analysis to a decade lower in Fourier frequency and half a decade higher in Fourier frequency as compared with most previous observations. Cyg X-1 showed rms variability $\approx 30\%$ characterized by a power spectral density (PSD) that was nearly flat between 0.02 and 0.2 Hz. The PSD was approximately $\propto f^{-1}$ between ≈ 0.2 and 2 Hz, while the power-law index of the 2–90 Hz PSD was seen to increase from ≈ -1.7 to ≈ -1.4 between the lowest and highest energy bands. The coherence function, rarely presented for most previous observations (although see Vaughan 1991; Vaughan & Nowak 1997; Cui et al. 1997), was remarkably close to unity over a wide range of frequencies. We also considered the Fourier frequency-dependent time delay between soft and hard photons.

As discussed in Paper II, hard photons in Cyg X-1 are seen to lag behind soft photons with a time delay that is dependent on Fourier frequency (see also Miyamoto & Kitamoto 1989; Miyamoto et al. 1992; Cui et al. 1997; Crary et al. 1998). Comparing the (0–3.9 keV) band with the (14.1–45 keV) band, the time delays are approximately $\propto f^{-0.7}$ and range from $\approx 2 \times 10^{-3}$ to 0.05 s. A more detailed study of these time delays will be the focus of this work. Specifically, we wish to understand what leads to this factor of 20 range in timescales, and we consider models where the time lags are created within the outer accretion disk (§ 2), created via photon diffusion in an extremely large corona (§ 3), or are due to wave propagation (§ 4).

As the basis for our discussions, we will for the most part take as our straw man model the "sphere + disk" Comptonization model that we considered in Paper I. We illustrate the geometry of this model in Figure 1. This model has a uniform coronal heating rate and nearly uniform density structure, but a nonuniform temperature structure. The seed photons for Comptonization are due to (reprocessed and direct) soft radiation from the outer, thin disk. This model does not include dynamical information. The advection-dominated accretion flow (ADAF) models have a similar geometry, as shown in Figure 1, but they

[1] JILA, University of Colorado, Campus Box 440, Boulder, CO 80309-0440; mnowak@rocinante.colorado.edu, dove@rocinante.colorado.edu, mitch@jila.colorado.edu.

[2] Institut für Astronomie und Astrophysik, Abt. Astronomie, Waldhäuser Strasse 64, D-72076 Tübingen, Germany; wilms@astro.uni-tuebingen.de.

[3] Space Radiation Laboratory, California Institute of Technology, MC 220-47, Pasadena, CA 91125; brian@srl.caltech.edu.

[4] Also CASA, University of Colorado, Campus Box 389, Boulder, CO 80309-0389.

[5] Also, Department of Astronomy, University of Colorado, Boulder, CO 80309.

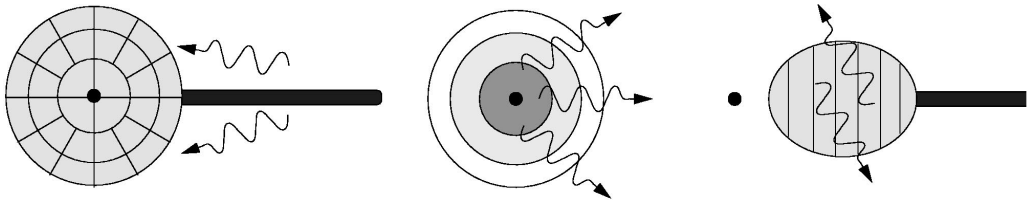


FIG. 1.—Geometries for recent models of Cyg X-1. Sphere+disk geometry, as considered by Dove et al. (1998) and Paper I (*left*). The seed photons for Comptonization come from the outer disk. The central corona has a uniform heating rate and seed electron density but a nonuniform temperature structure (cf. Dove et al. 1997a). Geometry considered by Kazanas et al. (1997) (*middle*). The seed photons for Comptonization are isotropic and arise from an unspecified source within the central region of the system. The corona has a spherical structure with a typically $R^{-3/2} \rightarrow R^{-1}$ density profile but uniform temperature structure. ADAF geometry (cf. Narayan 1996) (*right*). The seed photons for Comptonization are cyclo/synchrotron photons that originate within the advective inner region. A cylindrical symmetry approximation for the structure is often taken.

model the accretion dynamics as well (Abramowicz et al. 1995; Narayan & Yi 1994; Narayan 1996; Esin, McClintock, & Narayan 1997). For ADAFs, a substantial portion of the accretion energy is advected into the black hole, potentially at a large fraction of free-fall speeds, in the form of thermal energy. (The density profile of matter in free fall is $\propto R^{-3/2}$.) The advective inner regions also produce cyclo/synchrotron photons, which are assumed to be the seed photons for Comptonization. Another model that we shall discuss is the Comptonization model of Kazanas, Hua, & Titarchuk (1997, hereafter KHT; see also Boettcher & Liang 1998). This model postulates a large spherical corona with a radial density profile typically $\propto R^{-3/2} \rightarrow R^{-1}$ but uniform temperature structure. The seed photons for Comptonization are isotropic and can originate either within the central regions of the corona (KHT) or externally (Boettcher & Liang 1998). Note that these models do not consider detailed flow dynamics.

In order to understand how these models might lead to the observed time delays, let us consider some of their characteristic timescales. We shall take the fiducial radius of the corona (or inner, advective region) to be $R = 50GM/c^2$, with $M = 10\ M_\odot$. (We shall adopt $M = 10\ M_\odot$ throughout the rest of this paper.) We then have the following characteristic timescales. The radial light-crossing timescale, $t_{\rm LC}$, is 2.5×10^{-3} s, which is comparable to the shortest time lags. For an 87 keV Compton corona the radial sound-crossing time, $t_{\rm SC} = 5 \times 10^{-3}$ s. The free-fall timescale, $t_{\rm FF}$, relevant for the ADAF models, is 8.5×10^{-3} s and is proportional to $R^{3/2}$. All three of these timescales are mainly relevant for the shortest time delays. In order for them to be applicable to the longest time delays, one needs to consider a radius of $10^3 GM/c^2$ for the light-crossing timescale and a radius of $\approx 160GM/c^2$ for the free-fall timescale. (Some ADAF models do posit a large radius for the advective region; Narayan 1996; Esin et al. 1997.) A single one of these mechanisms can explain the observed dynamic range in time delays only if it samples a comparably large range in radii.

The viscous diffusion timescale is $\approx R^2/\nu$, where ν is the kinematic viscosity. Taking an α-disk model, $\nu \approx \alpha H c_s$, where H is the disk thickness and c_s is the speed of sound (cf. Frank, King, & Raine 1992). Using the speed of sound from our best-fit corona model and taking $H \approx R$ and $\alpha \approx 0.1$, the viscous diffusion time, t_D, is approximately 0.03 s, which is comparable to the longest time lags. The Keplerian period at $R = 50GM/c^2$ is $t_{\rm K} \approx 0.1$ s and is also comparable to our longest time delays. All of the above characteristic timescales, along with the observed time lags, are presented in Figure 2.

We see that there is a range of characteristic timescales comparable to both the shortest and longest observed time lags. The latter are perhaps the more difficult to understand theoretically. Two extremes for explaining the longest time lags are a small radius and a slow mechanism (e.g., viscous diffusion) or a fairly large radius and a fast mechanism (e.g., light or sound speed propagation). The fact that there is extremely high coherence between the soft and hard bands (cf. Paper II), even at frequencies near 0.1 Hz where we see the longest time delays, makes it unlikely that a combination of these two possibilities is at work. (Even individually coherent processes will appear incoherent when summed, unless each process yields the same transfer function from soft to hard; Vaughan & Nowak 1997.)

In this paper we consider both of the above possibilities. In § 2 we calculate the effect that coronal "reprocessing" has on time delays that are intrinsic to the soft X-ray seed photons. We explore this possibility, first discussed by Miller (1995) and Nowak & Vaughan (1996), using our best-fit coronal model of Paper I. In § 3 we consider the suggestion of KHT that the time delays are created by Compton scattering in a corona that extends several decades in radius. We present simple, phenomenological propagation models in § 4. We use these models to show that the time delays can have a complicated frequency dependence even

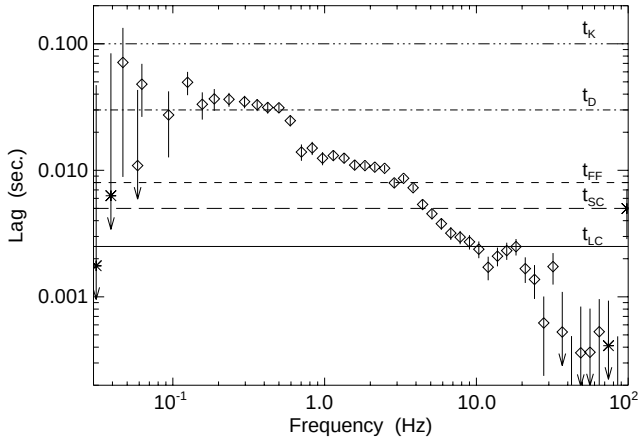


FIG. 2.—*RXTE* observations of time delays between the (0–3.9 keV) and (14.1–45 keV) light curves of Cyg X-1. Diamonds indicate where the hard lags the soft, and stars indicate where the soft lags the hard (Paper II). Lines represent characteristic timescales for a coronal radius of $50GM/c^2$ with $M = 10\ M_\odot$. The solid line is the radial light-crossing timescale ($t_{\rm LC}$); the long-dashed line is the radial sound-crossing time ($t_{\rm SC}$); the short-dashed line is the free-fall timescale ($t_{\rm FF}$); the dash-dotted line is the viscous diffusion timescale for a hot, geometrically thick cloud (t_D); and the dashed-triple-dotted line is the Keplerian orbital period for a thin disk ($t_{\rm K}$).

under very simple assumptions. We furthermore discuss the characteristic propagation speeds that such models imply. We present our conclusions in § 5.

2. TIME DELAYS INTRINSIC TO THE SEED PHOTONS

As discussed in Paper II (and references therein), one naturally expects that the hard photons lag the soft photons if the high-energy spectrum is mainly due to Comptonization. The time delay is due to the fact that the hard photons undergo several more scattering events than the soft photons. Such time delays should approximately depend on the logarithm of the energy (Paper II and references therein) and should be of order the light-crossing time of the corona. As was first pointed out by Miyamoto & Kitamoto (1989) and shown in Figure 2 above, this is considerably shorter than the longest observed delays.

This fact led Miller (1995) to suggest that the time lags might be intrinsic to the seed photons for Comptonization and that the input time delay's frequency dependence (although not amplitude) might be preserved by Comptonization. As discussed by Miller (1995) and elaborated on by Nowak & Vaughan (1996), the Fourier frequency dependence of the time delay is preserved, typically at low frequency, if the difference between the input and output photon energies is not too great. The amplitude of the time delay, however, tends to be *decreased* in the scattering process, perhaps substantially so (Nowak & Vaughan 1996). A constant time delay is introduced typically at high Fourier frequency. The amplitude of this time lag "shelf" is given by the difference of the mean diffusion times through the Compton cloud for the two energy bands being compared and thus should depend logarithmically on energy (Pozdnyakov, Sobol, & Sunyaev 1983; Miller 1995; Nowak & Vaughan 1996). In addition to the introduction of a constant time delay at high Fourier frequency, one also expects that the intrinsic PSD of the seed photons will be attenuated, especially at high frequency (Brainerd & Lamb 1987; Kylafis & Klimis 1987; Wijers, van Paradijs, & Lewin 1987; Stollman et al. 1987; Bussard et al. 1988; Kylafis & Phinney 1989; Miller & Lamb 1992; Miller 1995; Nowak & Vaughan 1996).

Given a source of seed photons and a Comptonization model, one can calculate these effects (Miller 1995; Nowak & Vaughan 1996). Take a discretely sampled seed photon light curve, $s_i^{[k]}$, where i denotes the time bin and $[k]$ denotes the energy band. The output light curve, $h_j^{[l]}$, is measured at times j and in energy band $[l]$. The two can be related by an equation of the form

$$h_j^{[l]} = \sum_k r_{ji}^{[lk]} s_i^{[k]} , \tag{1}$$

where $r_{ji}^{[lk]}$ describes the *linear* transfer properties of the Comptonizing medium in both time ($i \rightarrow j$) and energy ($[k] \rightarrow [l]$) (cf. Nowak & Vaughan 1996 and Appendix A below). The Compton corona can be described by such a linear transfer function if the coronal structure is *stationary*, which would also imply a unity coherence function measured between the output bands (Nowak & Vaughan 1996).

In Fourier space, equation (1) can be written as

$$H_m^{[l]} = \sum_k R_m^{[lk]} S_m^{[k]} , \tag{2}$$

where capital letters denote discrete Fourier transforms, m denotes the discrete frequency bin, and $R_m^{[lk]}$ is the transform of a *column* of $r_{ji}^{[lk]}$ (i.e., i held fixed and j free to vary; Nowak & Vaughan 1996). We can then relate the measured PSD and cross power spectrum (CPD) to the input PSD and CPD by

$$H_m^{[l]} * H_m^{[n]} = \sum_k R_m^{[lk]} * R_m^{[nk]} (S_m^{[k]})^2 + \sum_{j \neq k} R_m^{[lk]} * R_m^{[nj]} (S_m^{[k]} * S_m^{[j]}) . \tag{3}$$

Given a Comptonization model we can readily calculate $r_{ji}^{[lk]}$, which can then easily be Fourier transformed to yield $R_m^{[lk]}$. As described in Appendix A, we have calculated the transfer functions for our best-fit Comptonization model of Paper I. We use these transfer functions to assess the effect of our Compton corona model on an input white noise source with an *intrinsic* time delay between soft and hard photons that is $\propto f^{-1}$. In our model of Paper I, 25% of the seed photons comes from energies less than 40.4 eV, 50% comes from energies less than 115 eV, and 75% comes from energies less than 214.4 eV. We choose these three energies as seed photon energies, and furthermore we impose a constant Fourier phase lag of $\pi/2$ between the 214.4 and 115 eV variability, as well as between the 115 and 40.4 eV variability. The resulting phase lag of π between the 214.4 and 40.4 eV variability is the *maximum* allowed phase lag[6] between any two energy bands (see Nowak & Vaughan 1996; Paper II). We also choose the amplitude of the variability to be identical for all three seed photon energy bands.

In Figure 3 we present the result of passing such white noise variability through our Comptonization model of Paper I. As an example, we present theoretical time delays and PSD for the (2–4 keV) band compared with the (12–50 keV) band. (Neutral hydrogen column density is not included in these theoretical calculations of time delays.) We hold all parameters of the Comptonization model fixed, including the temperature of the seed photons from the disk, to the values of Paper I; however, we vary the physical radius of the corona. Specifically, we consider radii of $30GM/c^2$, $50GM/c^2$, $150GM/c^2$, and $500GM/c^2$. A number of results are immediately apparent from these figures.

First, the largest physically allowed phase lag between the 214.4 and 40.4 eV variability was still *too small* to reproduce the majority of the observed time delays. Thus, the hypothesis of Miller (1995) and Nowak & Vaughan (1996) that the time delays could be intrinsic to the disk appears to be wrong. As discussed by Nowak & Vaughan (1996), such a large input phase lag is required because of the great disparity between the input energy (≈ 150 eV) and the output energies (≈ 3, 20 keV).[7] The required input phase lag can be decreased if the temperature of the seed photons is increased; however, this is not allowed by the energy spec-

[6] By convention, the Fourier phase lags are taken to be in the range $[-\pi, \pi]$. Thus, a time delay that leads to a phase lag of $3\pi/2$ will be measured as a phase *lead* of $\pi/2$. We choose the maximum phase lag of π in order to determine the maximum possible output phase lag.

[7] Imagine that we have input energy bands, E_a and E_b, *each* of which scatter into two observed output bands, E_1 and E_2. If the input energy bands scattered into the output energy bands in equal proportion (i.e., $[E_a \rightarrow E_1]/[E_a \rightarrow E_2] = [E_b \rightarrow E_1]/[E_b \rightarrow E_2]$) then the *intrinsic* time delays would be completely wiped out. In reality, the scattering is slightly asymmetric, which allows a remnant of an input time delay to remain. If $E_a < E_b$ and $E_1 < E_2$, a slightly smaller proportion of E_a scatters into E_2, as compared with E_b that scatters into E_2. For fixed input energy bands, this asymmetry decreases with increasing output band energy, and hence the intrinsic time delays are more completely erased (cf. Nowak & Vaughan 1996).

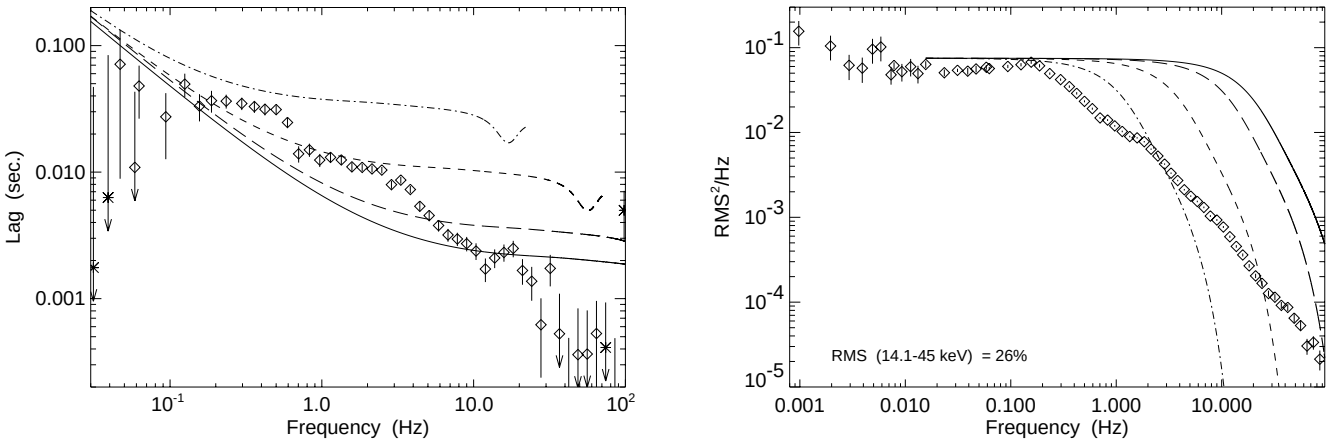


FIG. 3.—Diamonds and stars are the same time lags as shown in Fig. 2 (*left-hand panel*). Solid lines are the theoretical time delays between the (12–50 keV) and (2–4 keV) light curves, assuming that the seed photons for Comptonization have an intrinsic phase lag of π between the 40.4 and 214.4 eV light curves. (The intrinsic time lag in the seed photons is therefore $\propto f^{-1}$; see text.) Diamonds are the observed Cyg X-1 PSD in the (14.1–45 keV) band, compared with theoretical (12–50 keV) PSD for a white-noise input (arbitrary normalization) (*right-hand panel*). For both figures, the solid line represents a coronal radius of $R = 30GM/c^2$, the long-dashed line represents $R = 50GM/c^2$, the short-dashed line represents $R = 150GM/c^2$, and the dash-dotted line represents $R = 500\ GM/c^2$.

tral modeling (Paper I). Further argument against the hypothesis is garnered from the fact that the calculated time delays *do not* depend logarithmically on energy, contrary to the observations (Paper II and references therein). The theoretical model does show a logarithmic energy dependence at high Fourier frequency, where a shelf in the theoretical time delay is clearly seen; however, the energy dependence weakens for lower frequencies. As shown in Paper II (Fig. 12), the data show a logarithmic energy dependence even at 0.3 Hz. We are thus forced to the conclusion that the majority of the observed time delays, in one fashion or another, must be created within the corona if our basic model for the energy spectrum is correct. However, this is *not* the same as saying that the variability (PSD) must be directly created in the corona (cf. § 3).

We do expect one effect of Comptonization to remain, even if the time lags are created within the corona itself, namely the time lag shelf at high frequency. After one scatter, a photon has essentially lost all information as to the spatial location of its origin. Thus, whether the seed photons come from an outer disk or whether they are internal to the corona (such as for ADAF models that invoke cyclo/synchrotron seed photons; Narayan 1996; Esin et al. 1997), the difference in diffusion times to reach two different output energies will still lead to a time lag shelf. The shortest observed time lag should be no smaller than this theoretically expected shelf. Such shelves clearly are seen at high Fourier frequency in the theoretical models presented in Figure 3. They range from 2×10^{-3} s for $R = 30GM/c^2$ to 0.04 s for $R = 500GM/c^2$. The observational data, on the other hand, do show a flattening in the time delays in the 10–30 Hz range. If we take this as the upper limit to an allowed theoretical time delay, then the maximum allowed coronal radius for our model of Paper I is $\approx 30GM/c^2$. There is also an observed flattening of the time delay in the region of 0.7–3 Hz. If we take this as the upper limit to an allowed theoretical time delay, then the maximum allowed coronal radius is $\approx 150GM/c^2$.

Which of these observational limits should we choose, and why do we ignore the even shorter time delays above 30 Hz? As discussed in Paper II, the time delays above 30 Hz are especially subject to noise as both the PSD *and* the coherence function are decreasing in this regime. We again note that there is a "hardening" of the 2–90 Hz PSD with increasing energy (Paper II), coincident with this coherence loss. We postulated that this was indicative of additional, multiple variability components that were being created directly within the corona. One speculation would be that these timescales are probing flares that are "feeding" the corona on dynamical timescales. Without being able to identify the physical nature of these hypothesized extra variability components, we do not know what their intrinsic time delays are. We *do* know, however, that multiple uncorrelated variability components will lead to a loss of coherence and that the *net* observed time delay in such regions will be a combination of many intrinsic lags and possibly even leads (Vaughan & Nowak 1997; Paper II, § 3.1). Thus, an *incoherent* frequency range *can* have observed time delays *less* than the minimum theoretically expected time lag shelf.

We should then choose the maximum allowed theoretical time lag shelf to be the *minimum* time delay observed in a region of near unity coherence. For our observations of Cyg X-1, this would be at ≈ 10 Hz, and thus this limits us to a maximum coronal radius of $\approx 30GM/c^2$. This is consistent with the limits on the PSD as well (cf. Fig. 3). Such a small corona has little effect on the PSD in the 0.02–2 Hz regime, where PSDs for all five observed energy bands (Paper II) have roughly the same shape. We note, however, that based on the PSD alone, especially if the PSD above $\gtrsim 10$ Hz is contaminated by other sources of variability, a much larger coronal radius ($\approx 150GM/c^2$) is tolerated.

It is tempting to associate the various "flattened" regions (≈ 0.1–0.5 Hz, ≈ 0.7–3 Hz, and ≈ 10–30 Hz) seen in the time delays of Figure 3 with time lags shelves due to Comptonization. This would imply a Compton corona with characteristic radii of $\approx 30GM/c^2$, $\approx 150GM/c^2$, *and* $\approx 500GM/c^2$. The (nearly) uniform density coronal model of Paper I *cannot* produce such a range of time lags. However, recently KHT have proposed a coronal model with an R^{-1} density profile that *can* produce a broad dynamic range of time delays. We consider such models in the next section.

3. TIME DELAYS CREATED BY THE CORONA

In the model of KHT, as well as the models of Boettcher & Liang (1998), both the observed power spectral densities and time lags are the result of passing an *isotropically emitted* white noise (i.e., flat) spectrum through an extended Comptonizing medium with a power-law density profile. The case of $\rho \propto R^{-1}$ represents equal optical depth per decade of radius and therefore roughly equal probability of seed photons from an isotropic source scattering within any given radial decade. This leads to a power-law shape for the observed PSD, as opposed to the fairly sharp cutoff seen in Figure 3. Time delays are created by the difference in diffusion times through the corona for hard and soft photons. Photons that scatter over large radii will have their intrinsic high-frequency variability wiped out (as in Fig. 3); therefore, any observed high-frequency variability must be due to photons that scattered only within the inner radial regions. High-frequency variability thus exhibits short time delays between hard and soft photons. Low-frequency variability potentially can be observed from photons that have scattered over a large radius. Low-frequency variability thus exhibits longer time delays between hard and soft photons. The time delay at all Fourier frequencies is expected to increase as the logarithm of the ratio of the hard to soft energy, as is observed (cf. Paper II and references therein). For quantitative agreement with the observations, KHT require coronal radii of $\mathcal{O}(10^4 GM/c^2)$.

The main objection to this scenario is that the source of soft seed photons is not fully specified. *ASCA* observations of the hard/low states of Cyg X-1 (Ebisawa et al. 1996) and of GX339−4 (Wilms et al. 1998a) show evidence of a "soft excess" that is reasonably well modeled by a multicolor blackbody spectrum with a peak temperature of ~ 150 eV. This temperature is suggestive of—but not definitive evidence for—the inner edge of an accretion disk (the putative source of the seed photons, although see Narayan 1996; Esin et al. 1997) being at radii $\gtrsim 50GM/c^2$, as opposed to being at the center of the corona. Both of these sources, as well as several other low/hard state galactic black hole candidates (GBHCs) have shown evidence of *weak* and *narrow* Fe lines at 6.4 keV (Ebisawa et al. 1996; Wilms et al. 1998a). The properties of these lines[8] can be explained naturally in the sphere + disk geometry.

Does a corona with a power-law density profile, but with seed photons arising from a geometrically thin outer disk, still produce the characteristic PSD and time delays as described by KHT? To answer this question, we have created a grid of Comptonization spectra with the following properties. The heating per particle in the corona was taken to go as R^{-1} (i.e., proportional to gravitational energy release), the density was taken to go as R^{-1} (i.e., the density structure chosen by KHT), and the seed photons were taken to come from a multicolor blackbody spectrum, with peak temperature 150 eV, originating from a geometrically thin outer disk. We used the same Comptonization code as described by Dove, Wilms, & Begelman (1997a) and used in Paper I. Unlike the models of KHT, which were isothermal out to $\mathcal{O}(10^4 GM/c^2)$, our simulations include the derivation of the self-consistent temperature structure of the corona by balancing the local Compton cooling rate with the local heating rate (which was $\propto R^{-1}$). For typical parameter values, the temperature was about 72 keV above the pole of the corona and only 40 keV at the equator near the edge of the sphere. (This cooler temperature is due to the increased density of soft photons near the accretion disk.) We applied these models to our *RXTE* spectra of Cyg X-1 (cf. Paper I) and obtained a reasonable fit to the data (Fig. 4). We find a best-fit coronal optical depth of 2.9, with an average coronal temperature of 58 keV.

As described in Appendix A, we again used a linear Monte Carlo code (with the radial coronal structure taken from our best-fit nonlinear model, but excluding the pole-to-equator temperature gradient) to calculate the time-dependent transfer functions for seed photon energies to transit to observed hard X-ray energies. In an analogous manner to the calculation described in § 2, we used these transfer functions to determine the effect that the corona has on any variability inherent to the Comptonization seed photons. In Figure 5*a* we show the resulting time lags between soft and hard X-ray variability. In Figure 5*b* we show the resulting PSD assuming a white noise power spectrum for the variability of the seed photons. Here we take all the photons, an input blackbody with temperature $kT = 150$ eV, to have a uniform initial Fourier phase. In both of these figures, we present results for coronal radii ranging from 30 to $500GM/c^2$.

Note that unlike the models of KHT and Boettcher & Liang (1998), we do *not* find time lags that are proportional to Fourier period and we do *not* find a PSD with a power-law dependence over a wide range of frequencies. Our results are qualitatively and quantitatively similar to the uniform (in density and heating) coronal models presented in Figure 3. Specifically, the resulting time lag is nearly constant as a function of Fourier frequency and is comparable to the light-crossing time across the diameter of the entire corona. The resulting PSD (assuming a white noise input) has a sharp cutoff as opposed to a power-law shape.

The major difference between the model presented here and those of KHT and Boettcher & Liang (1998) is one of geometry. The latter models assume an isotropic source of seed photons. The models of KHT assume that the seed photons originate from the interior to the corona, while the models of Boettcher & Liang (1998) consider both internal and external illumination of the corona. Both models assume isotropic illumination. The core of the corona, where the photons can undergo the scatters on the shortest timescales and thus not suffer substantial losses of high-frequency variability power, is initially visible to the seed photons in these models.

In our model, where the seed photons originate in a geometrically thin disk exterior to the corona, the central core of the corona subtends a very small solid angle as viewed by the disk. The photons emanating from the disk do not isotropically illuminate the corona. This geometry, coupled with the fact that our best-fit model is mildly optically thick, means that a substantial fraction of the photons must first scatter on the large radii of the outer corona before being able to scatter within the inner radii of the corona. Thus, the time lags are dominated by the *longest* time delays at *all* Fourier frequencies.

[8] Note that if the energy release from the corona is centrally concentrated, as in the ADAF models or the coronal model with R^{-1} heating described below, then the Fe line places *upper limits* to the coronal radius (cf. Esin et al. 1997). The fact that Fe lines are seen with equivalent widths ≈ 30–40 eV, even in very low luminosity observations of GBHC such as Nova Muscae (Zycki et al. 1998) and GX339−4 (Wilms et al. 1998), tends to argue against very large radii in the sphere + disk geometry.

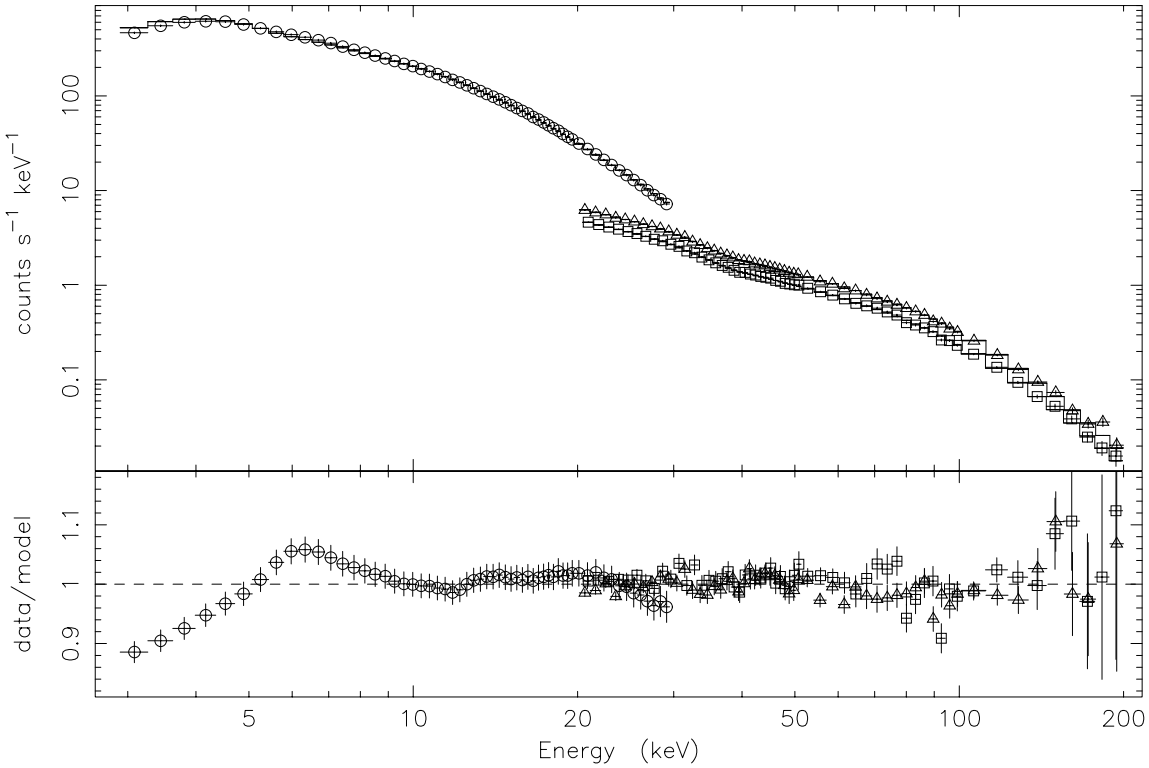


FIG. 4.—Best-fit sphere + disk Comptonization model to *RXTE* data of Cyg X-1. (Circles are PCA data, triangles and squares are HEXTE data; cf. Paper I.) Unlike the Comptonization models presented in Paper I, here the heating rate per particle is $\propto R^{-1}$ and the coronal density structure is $\propto R^{-1}$. The best-fit parameters were a total optical depth of 2.9 and an average coronal temperature of 58 keV. The reduced χ^2 for the fit was 1.75. As discussed in Paper I, a possible reason for the residuals in the 3–7 keV region (which are slightly larger than the systematic uncertainties in the PCA) is our assumption of a sharp transition from thin, cold disk to thick, hot corona.

Further differences with our model are that we consider coronal heating $\propto R^{-1}$, we allow reprocessing of hard X-ray photons in the geometrically thin, outer accretion disk, and we allow for anisotropic temperatures in the corona (although in the linear Monte Carlo code we only include the radial temperature gradients). We conjecture that the primary reason the results of KHT (who use a uniform coronal temperature of 50 keV and optical depth of $\tau = 2$) are so drastically different is precisely because of their choice of an isotropic source of seed photons. (Boettcher & Liang 1998 show that results qualitatively similar to those of KHT are obtained even if the isotropic source of seed photons is exterior to the corona.) Again, the physical nature of this source is not fully described in the work of KHT. However, such a seed photon source geometry is qualitatively similar to that predicted by ADAF models (Narayan 1996; Esin et al. 1997). In our model the seed photons only "isotropize" (as viewed by the corona) after scattering on large radii and therefore always exhibit the longest time delays.

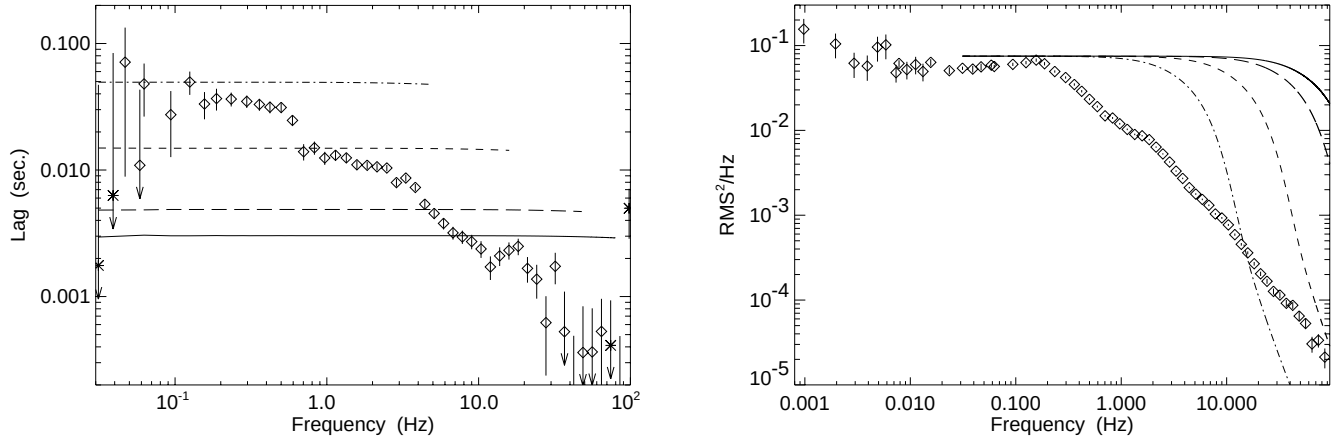


FIG. 5.—Diamonds and stars represent the same time lags as shown in Fig. 2 (*left-hand panel*). Lines are the theoretical time delays between the (14.1–45 keV) and (1–3.9 keV) light curves assuming that the seed photons originate in the geometrically thin outer disk and have a temperature of $kT = 150$ eV. Diamonds are the observed Cyg X-1 PSD in the (14.1–45 keV) band (*right-hand panel*). Lines are the theoretical PSD for the (14.1–45 keV) band assuming that the $kT = 150$ eV seed photons have a white noise power spectrum (arbitrary normalization). For both figures, the solid line represents a coronal radius of $R = 30GM/c^2$, the long-dashed line represents $R = 50GM/c^2$, the short-dashed line represents $R = 150GM/c^2$, and the dash-dotted line represents $R = 500GM/c^2$.

4. PROPAGATION MODELS

It has been suggested that the observed variability in Cyg X-1 can be produced in the context of ADAF models by disturbances propagating from the cold, outer disk into the hot, advection-dominated inner region (Manmoto et al. 1996). Manmoto et al. (1996) considered the inward propagation, and advection, of a large-amplitude, cylindrically symmetric disturbance. The basic concept of an inward-propagating wave presented in Manmoto et al. (1996) is an intriguing one. If the cold outer disk, which is not *directly* observed by *RXTE*, is the source of disturbances *and* the inner region then responds to these disturbance in a *linear* fashion, then we expect there to be unity coherence between hard and soft photons (Vaughan & Nowak 1997). As also discussed by Vaughan & Nowak (1997), two-dimensional waves can reproduce some of the qualitative features of the observed time delays.

The work of Manmoto et al. (1996) was not directly applicable to Cyg X-1, however, as it only considered modulation of the thermal bremsstrahlung emission, which is essentially negligible in ADAF models, and it did not quantitatively address the lags between hard and soft X-ray photons; and their model only produced modulation on order of the advective timescale and not on the broad range of timescales required to explain the Cyg X-1 PSD. The basic concept, however, is worth considering further. Lacking a dynamical theory associated with our Comptonization models, we explore below the notion of propagating disturbances via the use of simple phenomenological models.

We consider two-dimensional waves not only because they are naturally suggested by a disk geometry (i.e., the hypothesized source of disturbances), but also because even in the absence of any dispersive mechanisms, two-dimensional waves do not satisfy Huygen's principle (cf. Morse & Feshbach 1953). This means that even in a nondispersive medium with uniform propagation speed, we do not expect there to be a constant time lag between hard and soft photons (cf. Paper II, § 5.1; Vaughan & Nowak 1997). A "cylindrical-symmetry" approximation has also been used for the inner advective regions of ADAF models (cf. Narayan 1996; Esin et al. 1997 and references therein). Note for the discussion that follows, much of the qualitative behavior that we describe is specifically related to the two-dimensional nature of the waves. We therefore would not expect the behavior described below, for example, if the waves originated in a geometrically thick outer disk.

For simplicity, we shall consider waves propagating cylindrically symmetrically in a medium with a *uniform* propagation speed. Furthermore, we shall consider waves that propagate inward toward a "sink" located at the origin. Take a disturbance, $\Psi(\boldsymbol{x}, t)$, that obeys the wave equation

$$\left(\frac{\partial^2}{\partial \boldsymbol{x}^2} - c_p^{-2}\frac{\partial^2}{\partial t^2}\right)\Psi(\boldsymbol{x}, t) = -4\pi\rho_S(\boldsymbol{x}, t)\,. \tag{4}$$

The sink at the origin is represented by $\rho_S(\boldsymbol{x}, t)$, which we take to be $\equiv\delta(\boldsymbol{x})\rho_S(t)$. That is, we will consider waves that propagate inward from the (unobserved) outer disk and then are absorbed at the origin *without* reflection.

We can relate the disturbance, Ψ, to the sink, ρ_S, via an advanced Green's function (Morse & Feshbach 1953; Vaughan & Nowak 1997). Furthermore, let us take the *observed* soft and hard light curves, $s(t)$, $h(t)$, to be the disturbance, $\Psi(\boldsymbol{x}, t)$, multiplied by response functions, $g_s(\boldsymbol{x})$, $g_h(\boldsymbol{x})$, integrated over the disk. Given these assumptions, the observed soft X-ray light curve becomes

$$\begin{aligned} s(t) &= (2\pi)^{-1}\int d\boldsymbol{x}\, g_s(\boldsymbol{x})\Psi(\boldsymbol{x}, t) \\ &= (2\pi)^{-1}\int dt'\rho_S(t')\int dr\, df\, r g_s(r)G_f(2\pi f, r)\exp(-i2\pi f\tau)\,, \end{aligned} \tag{5}$$

and similarly for $h(t)$. In equation (5) we have taken the sink to be a delta function at the origin, we have taken the soft light curve response to be cylindrically symmetric, and we have written the Green's function, G_f, in Fourier space (cf. Morse & Feshbach 1953). We do this because we wish to calculate the time delays as a function of Fourier frequency.

Using the convolution theorem (cf. Morse & Feshbach 1953), we write $S(f)$, the Fourier transform of $s(t)$, as

$$S(f) = \frac{P_S(f)}{2\pi}\int dr\, r g_s(r)G_f(2\pi f, r)\,, \tag{6}$$

where $P_S(f)$ is the Fourier transform of $\rho_S(t)$. We obtain a similar expression for $H(f)$, the Fourier transform of the hard X-ray light curve.

The Fourier transform of $t_r(\tau)$, the transfer function between soft and hard X-rays (cf. Paper II), is then just the ratio between $H(f)$ and $S(f)$. That is,

$$T_r(f) = \frac{\int dr\, r g_h(r)G_f(2\pi f, r)}{\int dr\, r g_s(r)G_f(2\pi f, r)}\,. \tag{7}$$

Note that the above does not depend on $P_S(f)$. That is, we can know the relative amplitude and phase of $S(f)$ and $H(f)$ without actually knowing their absolute values individually. Furthermore, if g_s, g_h, and G_f do not vary with time, then $T_r(f)$ is constant and coherence is preserved (Vaughan & Nowak 1997; Paper II). For propagation models such as this, the observed Fourier phase delay is simply the Fourier phase of equation (7), while the time delay is this phase divided by $2\pi f$.

Here we point out several caveats associated with the validity of equations of the general form of equation (7). Linearity of the waves is essential. Inherent in our assumption of linearity is that the accretion system *locally* produces radiation in response to the wave and that the waves themselves do not produce X-rays in the outer regions of the disk. If the waves steepen into shocks, as for the disturbances discussed by Manmoto et al. (1996), then a transfer function formalism will *not* be valid. Furthermore, the coherence function for such a case would not be close to unity, contrary to the observations (Paper II; Vaughan & Nowak 1997). Even with the assumption of linearity, we are further relying on the assumption of cylindrical symmetry. There cannot be too large a variation of phase along the azimuthal direction of the wave front, or else the inward-propagating wave fronts will add incoherently. (Vaughan & Nowak 1997 show that individually coherent, linear processes can produce a net observed incoherent process when added incoherently in such a manner. Nowak et al. 1998b discuss how such a sum of coherent processes can be used to reproduce the small-amplitude deviations from unity coherence seen in the light curve of the BHC GX 339−4.) We shall now consider a specific example of a simple phenomenological model for wave propagation, with parameterized

responses of the soft and hard X-rays, that qualitatively reproduces the time delays observed in Cyg X-1. This model also gives us insight into the quantitative limits that one might be able to set on the disturbance propagation speeds from combined dynamical/spectral models. Taking a constant propagation speed, and solving equation (4) in terms of separate Fourier components (cf. Morse & Feshbach 1953), the Fourier transform of the two-dimensional Green's function becomes

$$G_f(2\pi f, r) = i\pi H_0^{(2)}(kr) , \tag{8}$$

where $k^2 \equiv (2\pi f/c_p)^2$ and $H_0^{(2)}$ is the second Hankel function of order zero. The second Hankel function has the appropriate type of singularity at the origin and is the relevant function for waves traveling toward the origin (Morse & Feshbach 1953).

For illustration, let us take $g_s(r)$ and $g_h(r)$ to be given by

$$g_s(r) \propto \theta\left(\frac{r - 6r_0}{r_0}\right) \exp\left(-\alpha_s \frac{r}{r_0}\right),$$
$$g_h(r) \propto \theta\left(\frac{r - 6r_0}{r_0}\right) \exp\left(-\alpha_h \frac{r}{r_0}\right), \tag{9}$$

where $\theta(x)$ is a step function and α_s, α_h, and r_0 ($\equiv GM/c^2$, $M = 10\ M_\odot$) are constants. We shall consider two sets of parameter values: ($\alpha_s = 0.06$, $\alpha_h = 0.024$) and ($\alpha_s = 0.06$, $\alpha_h = 0.048$). With these parameters, 95% of the soft photons come from $r \lesssim 50r_0$ and 95% of the hard photons come from $r \lesssim 20r_0$ and $r \lesssim 40r_0$, respectively. The resultant phase lags then depend on c_p, the propagation speed of the disturbances.

Results for this model and several different propagation speeds are presented in Figure 6. As can be seen from the figure, this phenomenological model qualitatively reproduces the functional form of the observed time lags. This is not surprising in that the two-dimensional wave propagation Green's function has properties similar to the "constant phase lag" transfer function described in Paper II (§ 4.1, eq. [11]). Specifically, the constant phase lag transfer function was seen to be a delta function plus a τ^{-1} tail (i.e., most photons are simultaneous, with a fraction of the hard photons lagging behind). The two-dimensional wave Green's function in the time domain is given by a step function, propagating at speed c_p, followed by a $\tau^{-1/2}$ tail (cf. Morse & Feshbach 1953). As we have taken the wave to propagate cylindrically symmetrically from the outside in, and we have taken the soft response to extend to larger radii than the hard response, the hard naturally lags the soft. If progressively higher energy responses have progressively smaller radial extents, the time lags will increase with energy. As the energy generation in a disk goes as R^{-1}, this is not an unreasonable expectation.

The most interesting things to note about Figure 6 are the propagation speeds required to quantitatively reproduce the longest observed time delays. We see that propagation speeds of $\mathcal{O}(0.01c$–$0.1c)$ are required, depending on the degree of overlap between the soft and hard X-ray response. As discussed in § 1, this is much slower than expected for Compton scattering, sound speed propagation, or gravitational free fall. The required velocity is increased if the degree of overlap between hard and soft response is decreased and/or if the overall radial extents of the responses are increased. For the former possibility, we note that we present a model where the radial extents of the hard and soft region differ by a factor of 2.5 and still the required propagation speed is quite low. For the latter possibility, it is unlikely that we can greatly increase the overall radial extents of the responses and still have sufficient high-frequency variability in the source of the disturbances. As discussed in Paper II, the PSD has the same functional form out to ≈ 2 Hz in all energy bands. Therefore, the source of variability (i.e., the initial inward-propagating waves) must have power out to at least this frequency. If we consider the dynamical timescale, this corresponds to a radius of $135GM/c^2$. Thus, it is unlikely that we can increase the radius, and thereby increase the required propagation speed, by more than a factor of 2 or 3. We note that we have tried functional forms for the response functions (such as step functions) different than those presented in equation (9). The results are qualitatively and quantitatively very similar.

5. SUMMARY

In previous papers we have presented analyses of *RXTE* data of Cyg X-1, where we have discussed spectral models

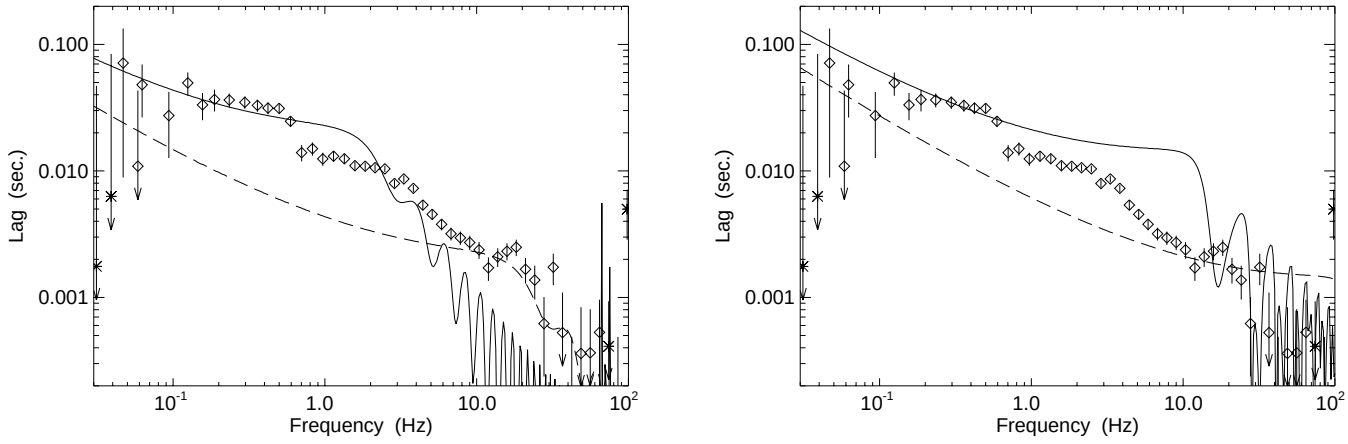


FIG. 6.—Diamonds and stars represent the same time lags as shown in Fig. 2 (*left-hand panel*). Lines are the theoretical time delays from simple phenomenological propagation models; 95% of the soft response comes from $r \lesssim 50GM/c^2$, and 95% of the hard response comes from $r \lesssim 40GM/c^2$ ($\alpha_s = 0.06$, $\alpha_h = 0.048$). The solid line is the theoretical time lag for $c_p = 0.01c$, and the dashed line is for $c_p = 0.1c$. On the right, 95% of the soft response comes from $r \lesssim 50GM/c^2$, and 95% of the hard response comes from $r \lesssim 20GM/c^2$ ($\alpha_s = 0.06$, $\alpha_h = 0.024$) (*right-hand panel*). The solid line is the theoretical time lag for $c_p = 0.06c$, and the dashed line is for $c_p = 0.6c$.

(Paper I) and timing analysis (Paper II). For the spectral models we concentrated on sphere + disk Comptonization models, as illustrated in Figure 1. Such models were found to provide a reasonably good description of the data over a broad energy range (3–200 keV). In Paper II we presented PSDs, the coherence function between hard and soft variability (cf. Vaughan & Nowak 1997), and the Fourier frequency-dependent time delay between hard and soft variability. In this work we considered this time delay in light of our sphere + disk Comptonization models for the spectrum.

The simplest expectation, as first noted by Miyamoto & Kitamoto (1989), is that time delays between hard and soft photons should be due to differences in diffusion times through the Compton corona and should be nearly *independent* of Fourier frequency. This is counter to the observations (Paper II, and references therein), which led Miller (1995) and Nowak & Vaughan (1996) to suggest that perhaps the time delays are intrinsic to the disk and are merely "reprocessed" by the corona. We explored this possibility with our Comptonization models and found this *not* to be the case. The required input phase lags are unphysically large ($\gtrsim \pi$), and furthermore the resulting time delays do not have the required logarithmic energy dependence (cf. Paper II and references therein). This is the chief conclusion of our paper: if the basic sphere + disk Comptonization geometry is correct, then the time delays must be created directly within the corona.

We then explored whether a corona with a power-law structure could reproduce the observed time delays, as was first suggested by KHT. As opposed to this work, which utilized an isotropic, central source of soft seed photons, we again considered the sphere + disk geometry. The seed photons in this case come from the geometrically thin, outer disk and therefore are *not* isotropic. The seed photons must first scatter on the largest radii of the corona before they can be viewed quasi-isotropically by the inner regions of the corona. We found that this sphere + disk geometry, even with a power-law density profile, therefore does not reproduce either the observed PSD or the observed time lags. We conjecture that an isotropic source of seed photons, as viewed by the corona, is required in order to create time lags in the manner suggested by KHT.

KHT do not have a fully self-consistent model for the source of the soft seed photons; however, their geometry is qualitatively similar to that of the ADAF models (cf. Narayan 1996; Esin et al. 1997), which use synchrotron photons from within the advective flow as the seed photons for Comptonization (Fig. 1). As for the models of KHT, the ADAF models can require a very large coronal radius. Such a large radius, however, poses problems with interpreting the observed spectra of GBHCs. Specifically, one typically sees a soft excess with characteristic temperatures of $kT \approx 150$ keV (possible evidence of the accretion disk), as well as weak, narrow 6.4 keV iron lines with equivalent widths of $\mathcal{O}(30$ keV) (Ebisawa et al. 1996; Zycki, Done, & Smith 1998; Wilms et al. 1998b). ADAF models predict[9] lower characteristic temperatures for any soft excess as well as smaller equivalent widths for the iron line, if the radius of the advective region is as large as the $\mathcal{O}(10^4 GM/c^2)$ required to reproduce the longest time lags.

If we take the *minimum* time delay (observed in a region where the hard and soft variability are *coherent* with each other) as indicative of the *maximum* allowed coronal radius, then *the corona must have a small*[10] radius $\lesssim 30GM/c^2$. This led us to explore the possibility that the time delays are related to propagation of cylindrically symmetric linear disturbances through a small corona. (Such "propagation models" have been considered by Manmoto et al. 1996, for example, but see our comments in § 4 above.) We concluded that if the corona is small and the time delays are due to linear disturbances propagating cylindrically symmetrically through the corona, then the propagation speeds are extremely slow. Such slow propagation speeds are likely inconsistent with ADAF models with advective region radii $\lesssim 150GM/c^2$.

The advent of *RXTE* allows us to obtain a very broad band spectrum ($\approx$3–200 keV) and simultaneously allows us to obtain temporal data on timescales comparable to the dynamical timescales of the very innermost regions of GBHC systems. The spectral capabilities of *RXTE* have demanded an increasing level of sophistication from Comptonization models. Combining the spectral data with the temporal data now requires us to consider the *dynamical* structure of Comptonization models as well. Currently there are two broad classes of models for the observations: ADAF models and similar coronal models with large radii (e.g., KHT) or sphere + disk models with fairly small radii and (here hypothesized) relatively slow "propagation speeds" in the coronal region. The former models require further study to show that they agree with *all* aspects of the spectral data (and the ADAF models require further work to demonstrate that they agree with the temporal data as well), whereas the latter models, which are purely spectroscopic in nature at the moment, need to be coupled with a viable dynamical theory. Further *RXTE* observations—coupled with future observations from instruments such as AXAF and/or XMM to study the details of the soft excesses and the weak, narrow iron line features—will likely be required to determine which of the above possibilities, if any, is the most promising model for Cyg X-1 and other similar GBHCs.

We would like to acknowledge useful discussions with O. Blaes, P. Michelson, E. Morgan, K. Pottschmidt, R. Staubert, M. van der Klis, and W. Zhang. This work has been financed by NSF grants AST91-20599, AST95-29175, INT95-13899, NASA Grants NAG5-2026, NAG5-3225, NAGS-3310, DARA grant 50 OR 92054, and by a travel grant to J. W. from the DAAD.

[9] There has been discussion at recent scientific meetings of the possibility of adding "cold blobs" of matter into the inner advective region of ADAF models in order to reproduce the observed Fe line characteristics. Many questions are raised by such additions to the ADAF model, such as what is the "natural" filling factor of the blobs? Will the additional cooling from the soft flux collapse the ADAF solution into a radiatively efficient state? Can a *narrow* Fe line, as is suggested by the data, be produced by blobs being advected with the flow? Will variability associated with blobs moving over a large range of radii still produce near-unity coherence between soft and hard radiation as is observed? Considering these issues is beyond the scope of this current work.

[10] Such a small radius is also suggested by the timing analysis that we presented in Paper II. Specifically, the slope of the high-frequency ($\gtrsim$3 Hz) PSD was seen to flatten with increasing photon energy (possibly indicative of "feeding" the corona on dynamical timescales at radii $\lesssim 50GM/c^2$). Also, the coherence was seen to drop at low frequency ($\lesssim$0.02 Hz; possibly indicative of the viscous timescale of the cool, thin accretion disk at radii $\gtrsim 50GM/c^2$), as well as at high frequency ($\gtrsim$10 Hz).

APPENDIX A

TIME LAGS IN THE SPHERE+DISK GEOMETRY

The major spectral results presented in Paper I and Paper II were based on models obtained using our nonlinear Monte Carlo code (cf. Dove et al. 1997b and references therein). It is very CPU time consuming and difficult to use such a code to perform a study of the temporal behavior of the sphere+disk geometry. We therefore used a separate linear Monte Carlo code for the computation of the shots presented in this paper.[11] The linear code is based on algorithms presented by Marchuk et al. (1980), Pozdnyakov et al. (1983), and Hua (1986, 1987). Compton scattering is simulated using the relativistic scattering formulae. The differential Klein-Nishina cross section is used in the computation of the scattering angle. The electrons are assumed to have a relativistic Maxwellian distribution, the effect of which is taken into account in the simulation of the Compton scattering and in the simulation of the mean free path of the photon. The code also includes the interaction of the radiation with cold matter, by making use of the fits to the photoabsorption cross sections for the first 30 elements given by Verner & Yakovlev (1995), Verner et al. (1993), and Band et al. (1990). Fluorescent line emission of the Fe Kα (6.4 keV), Fe Kβ (7 keV), Si Kα (1.7 keV), and S Kα (2.3 keV) lines was included in the simulations using the theoretical fluorescence yields published by Kaastra & Mewe (1993).

In order to reduce the statistical noise in the emerging spectrum and in order to have a good coverage of the higher order Compton scatterings, the method of weights was used. In this method, a photon starts out with a weight $w = 1$. After each propagation step the optical depth τ to the boundary of the system is computed. The probability that the photon escapes without further scatterings is $P = \exp(-\tau)$. Therefore, a photon with weight $w \exp(-\tau)$ is added to the output spectrum and the rest of the photon, with weight $w[1 - \exp(-\tau)]$, continues to scatter within the corona. After a photon gets photoabsorbed within the accretion disk, it gets reemitted with a new weight given by Yw, where Y is the fluorescence yield of the absorbing element and w is the weight of the photon before the absorption and its energy E is set to the fluorescence energy of the fluorescence line. The photon is killed if its weight goes below a threshold, usually taken to be 10^{-6}. We refer to Pozdnyakov et al. (1983), Górecki & Wilczewski (1984), and White, Lightman, & Zdziarski (1988) for a more in-depth description of the method of weights.

A photon emitted from the sphere can hit the disk and vice versa. These photons are temporarily stored and dealt with after the code has finished with following the "primary photon." For a correct computation of the spectrum emerging from the sphere+disk geometry, energy conservation of the initial photon has to be taken into account. Each photon escaping the sphere and hitting the accretion disk deposits an energy wE within the disk, where E is the photon energy and w is again its statistical weight. A fraction of this energy subsequently escapes the system in the form of Compton-reflected radiation or fluorescence lines. The rest of the deposited energy is thermalized and finally reemitted in the form of one or more blackbody photons at the position where the original incident photon hit the disk.

Thermalization in the accretion disk occurs primarily via photoabsorption of a photon followed by the emission of either a photoelectron or an Auger electron. The typical energy for these electrons is on the order of a few keV or less. The electron then loses its energy primarily via Coulomb interactions with other electrons. The typical relaxation timescale for thermalization is given by (Frank et al. 1992, eq. [3.32])

$$t \sim \frac{me^2v^3}{8\pi N_E e^4 \ln \Lambda} \frac{mev^2}{2kT} = \frac{me^{1/2}}{2^{3/2}\pi e^4 \ln \Lambda} \frac{E^{5/2}}{N_E kT} \sim 10^{-5} \text{ s} \left(\frac{E}{10 \text{ keV}}\right)^{5/2} \left(\frac{N}{10^{16}/\text{cm}^3}\right)^{-1} \left(\frac{kT}{1 \text{ keV}}\right)^{-1}, \quad \text{(A1)}$$

where $E = mev^2/2$ is the initial energy of the electron, N_E the electron number density, e the elementary charge, T the temperature of the plasma, and $\ln \Lambda \approx 15$ is the Coulomb logarithm. Since the thermalization timescale is small compared with the light-crossing time of the spherical disk and the light travel time from the accretion disk to the sphere, it can be assumed that the thermalization and Compton reflection occur quasi-instantaneously. Consequently, the time spent by the photons within the accretion disk was not taken into account in the determination of the time lag and the thermalized photons were considered to be reemitted at the time when they hit the disk. The effect of thermalization is to cause "echoes" in the temporal response of the system to an initial burst of photons, since the thermalized photons are again able to produce hard photons by Comptonization in the sphere.

In order to be able to study the effect of radially symmetric disturbances of the accretion disk on the temporal behavior of the emerging Comptonization spectrum we computed the Green's function for photons emitted from a ring of radius r. For this paper we take r to be twice the coronal radius. The *initial* seed photon energy distribution was taken to be a delta function at a prescribed energy (40.4, 115, and 214.4 eV for the simulations shown in Fig. 3; cf. § 2). Those Comptonized photons, however, that are subsequently reprocessed in the disk are taken to obey a multicolor blackbody spectrum with a prescribed maximum temperature (here, 150 eV) and radial temperature dependence $\propto R^{-3/4}$. We chose this procedure because we wished to consider the effects of Comptonization on phase lags intrinsic to the seed photons, and furthermore because the coronal structure in the linear code was *fixed* to that of our best-fit nonlinear model as presented in Paper I. For the computation of the time lag, the path length of the photon was integrated from its generation to the point where the photon was leaving the system. To avoid artificial phase lags introduced by the size of the system, this latter point was defined to lie on a sphere encompassing the whole system.

[11] In a linear Monte Carlo code, photons are propagated one at a time through a background medium with predefined properties, while in a nonlinear code, a multitude of particles is also used to simulate the interaction between the radiation field and the medium, as well as interactions between individual photons, such as photon-photon pair production.

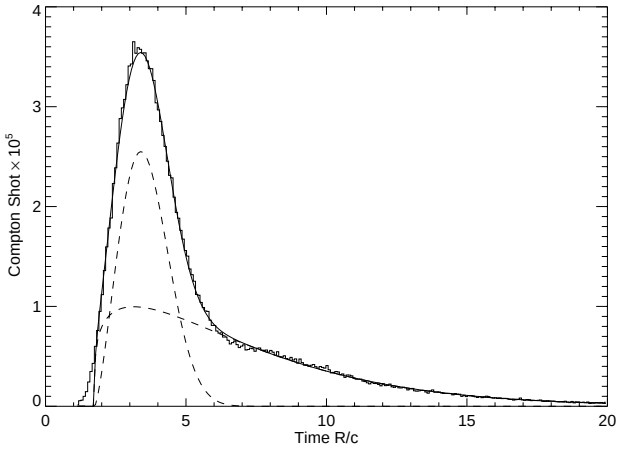


FIG. 7.—A Compton shot, for the Comptonization model of Paper I, fit with two Weibull functions with a common starting time. The x-axis is in units of the radial light-crossing time of the sphere, and the y-axis is the number of photons exiting the system in a restricted energy band at each time step.

The propagation of a large number (7.5×10^5) of photons was followed until their statistical weights were very small. (Nearly all photons had left the system within less than 30 light-crossing times.) A typical resulting output "Compton shot" is shown in Figure 7. Note that the shot has a narrow component occurring at early times and a broad component occurring at later times. This broad component is partly attributable to reprocessing in the disk; it is the "echo" mentioned above. Properly normalized, the total shot *is* the transfer function, $r_{ij}^{[lk]}$, described in equation (1). Taking Fourier transforms of such shots, we were able to derive the theoretical time delays of §§ 2 and 3. We took the Fourier transforms of analytic fits to the Compton shot profile in order to avoid spurious power, especially at high Fourier frequencies, due to numerical counting noise. We found that the combination of two generalized gamma distributions, specifically two Weibull distributions with a common start time, were excellent fits to *all* the shot profiles that we considered. A sample fit is shown in Figure 7. We describe these distributions in more detail in Appendix B.

APPENDIX B

GENERALIZED GAMMA AND WEIBULL DISTRIBUTIONS

The probability density function of the generalized Gamma distribution is given by

$$P_\Gamma(x;\,\alpha,\,\beta,\,\gamma) = \frac{\alpha}{\beta}\left[\Gamma\left(\frac{1+\gamma}{\alpha}\right)\right]^{-1}\left(\frac{x}{\beta}\right)^{\gamma}\exp\left[-\left(\frac{x}{\beta}\right)^{\alpha}\right] \text{ for } x > 0\,,$$
$$0 \text{ for } x \le 0\,, \tag{B1}$$

where

$$\Gamma(x) = \int_0^\infty t^{x-1}\exp\,(-t)\,dt \tag{B2}$$

is Euler's gamma function. The generalized gamma distribution is one of the most studied probability density functions of statistics since many of the important nondiscrete density functions can be derived from P_Γ. For example, $P_\Gamma(x;\,2,\,\sqrt{2\sigma},\,0)$ is the one-sided normal distribution, and $P_\Gamma(x;\,1,\,2,\,n/2-1)$ is the χ^2 distribution. The properties of the generalized Gamma distribution are discussed by Gran (1992) to whom the reader is referred for a more extensive discussion.[12] Note that the generalized gamma distribution used here is a generalization of the gamma distribution used by KHT, which has one parameter less.

In the special case of $\gamma = \alpha - 1$ the gamma distribution is called a Weibull distribution. This distribution was first used in 1939 by Waloddi Weibull as an empirical description for the distribution of the strength of materials to failure (Weibull 1939). Since then, the distribution has had a widespread use in many fields outside of engineering mechanics, e.g., to describe the mass distribution of crushed materials (Brown & Wohletz 1995), to describe the distribution of the force amplitudes exerted by ocean waves onto swimming platforms and oil rigs (Gran 1992), to describe the distribution of wind speeds to produce building codes (Whalen 1996), and many others.

[12] The notation used here is different from that used by Gran (1992). His notation can be mapped onto the notation used here by substituting $a \to (\gamma+1)/\alpha$, $h \to \alpha$, and $A \to \beta$.

The probability density of the Weibull distribution is given by

$$P_w(x;\,\alpha,\,\beta,\,x_1) = \left(\frac{\alpha}{\beta}\right)\left(\frac{x-x_1}{\beta}\right)^{\alpha-1} \exp\left[-\left(\frac{x-x_1}{\beta}\right)^{\alpha}\right] \qquad \text{for } x > x_1\ ,$$
$$= 0 \qquad \text{for } x \le x_1\ , \tag{B3}$$

where $\alpha,\ \beta > 0$. In many applications, the "threshold" or "location parameter" x_1 is implicitly set to zero (as has been done for the generalized gamma distribution above). For $\alpha > 1$ the Weibull distribution looks similar to an asymmetric "bell curve," while for $\alpha < 1$ the distribution resembles an exponentially decaying function. Since α determines the shape of the distribution, it is often called the "shape parameter." The parameter β is called the "scale parameter" since for a given α the variance of the distribution is uniquely defined by β.

The properties of the Weibull distribution are discussed fully by Gran (1992). For our fits of the Compton shots we combined two Weibull distributions, which were constrained to the same x_1. Thus, including the absolute normalization of $r_{ij}^{[lk]}$ and the relative normalization of the two distributions, we had seven fit parameters. This yielded excellent fits for all of the Compton shots considered for this work.

REFERENCES

Abramowicz, M., Chen, X., Kato, S., Lasota, J. P., & Regev, O. 1995, ApJ, 438, L37
Band, I. M., Trzhaskovskaya, M. B., Verner, D. A., & Yakovlev, D. G. 1990, A&A, 237, 267
Belloni, T., & Hasinger, G. 1990a, A&A, 227, L33
———. 1990b, A&A, 230, 230
Boettcher, M., & Liang, E. P. 1998, ApJ, submitted (astro-ph/9802283)
Brainerd, J., & Lamb, F. K. 1987, ApJ, 317, L33
Brown, W. K., & Wohletz, K. H. 1995, J. Appl. Phys., 78, 2758
Bussard, R. W., Weisskopf, M. C., Elsner, R. F., & Shibazaki, N. 1988, ApJ, 327, 284
Crary, D. J., Finger, M. H., Kouveliotou, C., van der Hooft, F., van der Klis, M., Lewin, W. H. G., & van Paradijs, J. 1998, ApJ, 493, L71
Cui, W., Zhang, S. N., Focke, W., & Swank, J. H. 1997, ApJ, 484, 383
Dove, J. B., Wilms, J., & Begelman, M. C. 1997a, ApJ, 487, 747
Dove, J. B., Wilms, J., Maisack, M. G., & Begelman, M. C. 1997b, ApJ, 487, 759
Dove, J. B., Wilms, J., Nowak, M. A., Vaughan, B. A., & Begelman, M. C. 1998, MNRAS, 298, 729 (Paper I)
Ebisawa, K., Ueda, Y., Inoue, H., Tanaka, Y., & White, N. E. 1996, ApJ, 467, 419
Esin, A. A., McClintock, J. E., & Narayan, R. 1997, ApJ, 489, 865
Frank, J., King, A., & Raine, D. 1992, Accretion Power in Astrophysics (2d ed.; Cambridge: Cambridge Univ. Press)
Górecki, A., & Wilczewski, W. 1984, Acta Astron., 34, 141
Gran, S. 1992, A Course in Ocean Engineering, Developments in Marine Technology 8 (Amsterdam: Elsevier)
Hua, X.-M. 1986, Ph.D. thesis, Univ. California, San Diego, La Jolla
———. 1997, Computers in Physics, vol. 11, 660
Kaastra, J. S., & Mewe, R. 1993, A&AS, 97, 443
Kazanas, D., Hua, X.-M., & Titarchuk, L. 1997, ApJ, 480, 280 (KHT)
Kylafis, N. D., & Klimis, G. S. 1987, ApJ, 323, 678
Kylafis, N. D., & Phinney, E. S. 1989, in Timing Neutron Stars, ed. H. Ögelman, & E. P. J. van den Heuvel (Dordrecht: Kluwer), 731
Manmoto, T., Takeuchi, M., Mineshige, S., Matsumoto, R., & Negoro, H. 1996, ApJ, 464, L135
Marchuk, G. I., Mikhailov, G. A., Nazaraliev, M. A., Darbinjan, R. A., Kargin, B. A., & Elepov, B. S. 1980, The Monte Carlo Methods in Atmospheric Optics, Springer Series in Optical Sciences 12 (Berlin: Springer)
Miller, G. S., & Lamb, F. K. 1992, ApJ, 388, 541
Miller, M. C. 1995, ApJ, 441, 770
Miyamoto, S., & Kitamoto, S. 1989, Nature, 342, 773
Miyamoto, S., Kitamoto, S., Iga, S., Negoro, H., & Terada, K. 1992, ApJ, 391, L21
Morse, P. M., & Feshbach, H. 1953, Methods of Theoretical Physics, Part I (New York: McGraw-Hill)
Narayan, R. 1996, ApJ, 462, 136
Narayan, R., & Yi, I. 1994, ApJ, 428, L13
Nowak, M. A., & Vaughan, B. A. 1996, MNRAS, 280, 227
Nowak, M. A., Vaughan, B. A., Wilms, J., Dove, J., & Begelman, M. C. 1998a, ApJ, 510, 874 (Paper II)
Nowak, M. A., Wilms, J., & Dove, J. B. 1998b, ApJ, in press
Pozdnyakov, L. A., Sobol, I. M., & Sunyaev, R. A. 1983, Astrophys. Rep., 2, 189
Stollman, G. M., Hasinger, G., Lewin, W. H. G., van der Klis, M., & van Paradijs, J. 1987, MNRAS, 227, 7
Vaughan, B. A. 1991, Ph.D. thesis, Stanford Univ.
Vaughan, B. A., & Nowak, M. A. 1997, ApJ, 474, L43
Verner, D. A., & Yakovlev, D. G. 1995, A&AS, 109, 125
Verner, D. A., Yakovlev, D. G., Band, I. M., & Trzhaskovskaya, M. B. 1993, Atomic Data Nucl. Data Tables, 55, 233
Weibull, W. 1939, A Statistical Theory of the Strength of Materials, Ingenior Ventenskaps Akademien Handlinger 151 (Stockholm: Generalstabens Litografiska Anstalts Förlag)
Whalen, T. M. 1996, Probabilistic Estimates of Design Load Factors for Wind-Sensitive Structures Using the Peaks over Threshold Approach, National Institute of Standards and Technology: Technical Report 1418 (Washington: US Govt. Printing Office)
White, T. R., Lightman, A. P., & Zdziarski, A. A. 1988, ApJ, 331, 939
Wijers, R. A. M. J., van Paradijs, J., & Lewin, W. H. G. 1987, MNRAS, 228, 17p
Wilms, J., Nowak, M. A., Dove, J. B., Fender, R. P., DiMatteo, T. 1999, ApJ, submitted
Wilms, J., Nowak, M. A., Heindl, W., & Pottschmidt, K. 1998b, in preparation
Zycki, P. T., Done, C., & Smith, D. A. 1998, ApJ, 496, L25